Development of Nanolaminate Thin Shell Mirrors

Gregory S. Hickey[a], Shyh-Shiuh Lih[a], Troy Barbee, Jr.[b]
[a]Jet Propulsion Laboratory, California Institute of Technology; [b]Lawrence Livermore National Laboratory, University of California

ABSTRACT

The space science community has identified a need for ultra-light weight, large aperture optical systems that are capable of producing high-resolution images of low contrast. Current mirror technologies are limited due either to not being scalable to larger sizes at reasonable masses, or to lack of surface finish, dimensional stability in a space environment or long fabrication times.

This paper will discuss the development of thin-shell, nano-laminate mirror substrates that are capable of being electro-actively figured. This technology has the potential to substantially reduce the cost of space based optics by allowing replication of ultra-lightweight primary mirrors from a master precision tool. Precision master tools have been shown to be used multiple times with repeatable surface quality results with less than one week fabrication times for the primary optical mirror substrate. Current development has developed a series of 0.25 and 0.5 meter spherical nanolaminate mirrors that are less than 0.5 kg/m^2 areal density before electroactive components are mounted, and a target of less than 2.0 kg/m with control elements. This paper will provide an overview of nanolaminate materials for optical mirrors, modeling of their behavior under figure control and experiments conducted to validate precision control.

1.0 INTRODUCTION

In order to meet the NASA goal of large (hundred of square meters), lightweight optics to enable future missions like Terrestrial Planet Finder, there is a need to change the paradigm regarding how large aperture optical structures are manufactured for space applications. The impact of this work is to develop a new class of enabling optical mirror substrates by breaking away from conventional optical materials. Current space optics are designed for ground-based testing in a 1 g environment using conventional materials. The most common is ultra-low thermal expansion glass (example Zerodur or ULE). This is the base technology for the Hubble Space Telescope. This approach has resulted in large, expensive, and heavy high-precision primary optics. Since Hubble, the 1-2 meter-class optics state-of-the-art has advanced to the current generation of light-weighted, non-actuated mirrors, generally fabricated from bonded or fused glass with complex core structures, with areal densities of 30-80 kg/m^2. Other programs are advancing the state of the art of large space optics. These include the Advanced Mirror System Demonstrator (AMSD), a joint NASA-DOD program developing lightweighted glass and beryllium mirrors (target areal density target of 15-20 kg/m^2). The next step is to develop lightweight optics that have integrated actuation and without a reaction structure.

The nanolaminate mirror program has developed a series of 0.25 and 0.5 meter spherical nanolaminate mirrors that are less than 0.5 kg/m^2 areal density before electroactive components are mounted, and a target of less than 2.0 kg/m with control elements. The continued development of nano-laminate mirrors will break the current paradigm of heavy, costly and long fabrication time primary optical mirrors for telescopes. This technology is directly applicable to both spherical and aspheric mirrors. Both would use the same fabrication process; where for non-spherical optics the only requirement would be a master aspheric precision tool. This technology is scaleable from the current 0.25 and 0.5 meter spherical mirrors currently being developed. In order to fabricate larger primary apertures, there would need to be a capitol investment for larger vacuum and deposition facilities. The practical limit for this technology is limited to several meters for the master tool. For tools greater than two meters, alternatives to Zerodur or ULE glass would have to be considered. Likely candidate materials include optics grade Silicon Carbide.

2.0 NANO-LAMINATE MATERIALS

Nano-laminates are a new class of materials (1,2,3) that are capable of approaching theoretical limits of strength. This property is important because high specific strength produces a more durable material at

smaller cross sectional areas. Additionally, as metals typically have stiffness larger than that characteristic of glasses, metallic nano-laminate materials will perform better as thin foil structures. Nano-laminates are synthesized using atom by atom physical vapor deposition magnetron sputtering(4,5,6). Elemental materials, alloys or compounds are sputtered producing individual layers having a thickness ranging from a single monolayer (0.2 nm) to hundreds of monolayers (>500 nm) Macroscopic sample thickness up to 400 μm has been demonstrated(7,8). We note here that the magnetron sputter deposition technology applied is a direct derivative of that applied to the deposition(9,10,11) of multilayer x-ray, soft x-ray and extreme ultra-violet reflecting optic structures. Thus high micro-structure perfection and uniformity is attainable as is required for exceptional mechanical performance.

Nano-structure or nano-phase materials are dense ultra-fine grained high interface concentration solids. Such materials are characterized by truly nano-scopic microstructures and thus, large interfacial area to volume ratios. Although multilayer or nano-laminate materials are not typically described by the terms nano-structure or nano-phase they are clearly high interface concentration nano-grained low contamination solids. The general nature of nano-laminate materials is widely known in the materials community as the ability to synthesize such materials for scientific study as developed at Lawrence Livermore National Laboratory (LLNL) has been applied at many nationally and internationally based laboratory's. At LLNL nano-laminates have been synthesized by magnetron sputter physical vapor deposition from layers of at least 83 of the 92 naturally occurring elements in elemental form, as alloys or as compounds with total thickness up to 400 μm and areas in excess of 3000 cm^2. The LLNL nano-laminate research, development and applications program has sought to bring this new class of matter into high payoff applications and then to broaden the application of the technologies developed to new areas. A general summary listing areas of application is given in TABLE 1. The listings in bold have been actively pursued at LLNL and applications developed and implemented.

TABLE 1: LLNL - ENGINEERED NANO-LAMINATE APPLICATIONS

<table>
<tr><td>ULTRA-HIGH STRENGTH MATERIALS</td><td>MAGNETIC TRANSDUCERS - GMR</td></tr>
<tr><td>HIGH PERFORMANCE TRIBOLOGICAL COATINGS</td><td>EUV, SOFT X-RAY AND X-RAY OPTICS SPECTROSCOPY</td></tr>
<tr><td>COATINGS FOR GAS TURBINE ENGINES</td><td>IMAGING AND MICROCIRCUIT LITHOGRAPHY DEVELOPMENT</td></tr>
<tr><td>ADVANCED COATINGS FOR MEDICAL APPLICATIONS</td><td>HIGH PERFORMANCE VISIBLE OPTICS</td></tr>
<tr><td>HIGH PERFORMANCE CAPACITORS FOR ENERGY STORAGE</td><td>NEW ENGINEERABLE SMART MATERIALS FOR SENSORS</td></tr>
<tr><td>CAPACITOR STRUCTURES FOR PROGRAMMATIC AND INDUSTRIAL APPLICATIONS</td><td rowspan="2">NEW MATERIALS AND NEW DEVICES BASED ON THE CHEMICAL & STRUCTURAL CONTROL AVAILABLE WITH ENGINEERED MULTILAYER MATERIALS</td></tr>
<tr><td>INTEGRATED CIRCUIT INTERCONNECTS</td></tr>
<tr><td>- MAGNETO-OPTIC READ/WRITE MEMORY</td><td>BASIS FOR NEW MANUFACTURING STRATEGIES</td></tr>
</table>

2.1 Nano-Laminate Thin Shell Mirrors Development

This large optic program represents a continuation of the science based application focus of the nano-laminate program at LLNL. This 18 year long LLNL effort has made LLNL the lead laboratory in the United States in nano-laminate development -and possibly the world. The current infrastructure for fabrication, characterization and application development efforts at LLNL along with the resident technical

expertise has made possible the production of the large diameter (25 cm and 50 cm), thick (up to 400 μm) free-standing structures being applied in this nano-laminate mirror development. Technically, three significant results specific to this application have been demonstrated:

1)First, large area (490 cm^2 and 980 cm^2) mechanically strong nano-laminate foils have been replicated more than 15 times from high quality figured mandrel tooling without degrading the mandrel quality
2) Active reflecting surfaces of the nano-laminate foils have been demonstrated to replicate the surface quality of the mandrel tooling with a surface roughness of 8 Å to 20 Å
3) Initial conceptual/engineering design of an advanced nano-laminate fabrication facility has been completed and has concluded that technology scale up to three meter diameter nano-laminate mirror structures can be successfully accomplished.

2.2 Nano-Laminate Structure

The micro-structural scale of nano-laminate materials is determined during synthesis by control of the thickness of the individual layers and interfacial chemical reaction of the two layers. These layers are from two monolayers (≈ 4 Å) to hundreds of monolayers (>5000 Å) thick and, except in special cases, generally define the in-plane grain size of the individual layers: The in-plane grain sizes are generally 2 or 3 times a individual layer thickness. It is important to note that atom-by-atom synthesis processes typically produce highly textured layers with the close-packed lattice plane of the layer materials in the plane of the multilayer. A cross-section transmission electron of a copper/zirconium nano-laminate microstructure developed for nano-laminate mirror applications is shown in Figure 1.

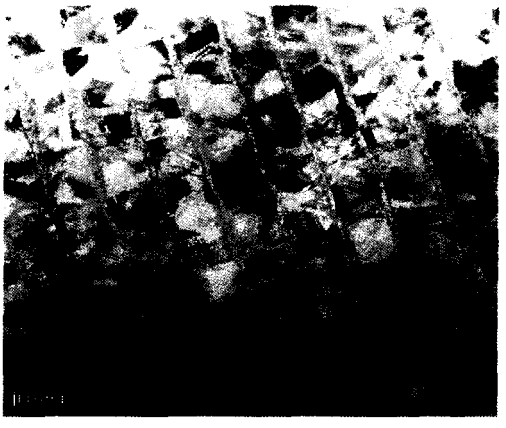

Figure 1. A cross-section transmission electron micrograph of a Cu/Zr nano-laminate is shown. The copper layers are ≈ 600 Å thick. The thinner layers (≈ 70 Å thick) are a amorphous copper-zirconium compound of approximate composition Cu_3Zr formed during sample synthesis.

The copper layers are ≈ 600 Å thick with an in layer grain size of ≈ 800 to 1000 Å. The thinner layers are an amorphous copper-zirconium alloy formed by a interfacial solid state amorphitization reaction during synthesis. The thickness of this layer is ≈ 80 Å. Its composition is approximately Cu_3Zr. These Cu/Zr nano-laminate materials are fully dense without structural flaws, other than those resulting from substrate or tooling contamination, defined by the nano-laminate period and the intrinsic mechanical properties of the component layers.

2.3 Nano-Laminate Mechanical Properties

These macroscopic nano-laminate materials have the potential for exceptional mechanical performance as a result of their nano-scopic microstructures and atomic distributions. Also, mechanically active flaws that limit mechanical performance are controllable so that the full potential of the structural control of the nano-laminate synthesis process is accessible. Studies of several material combinations in macroscopic multilayer form (25 μm thick) have substantiated this as shown in Table 2. The results are illustrative of the

potential of nano-laminate structures that result from the ability to synthesize materials at the limits of microstructure engineering by control of the synthesis conditions.

TABLE 2: Summary of selected mechanical properties of thick nano-laminate materials synthesized from high purity copper, 304 stainless steel, zirconium, platinum and chromium. Comparison with estimated strengths based on volume average of properties of individual layers[a] is also presented.

Material	Period (nm) Strength Improvement	Hardness (meas.)	Strength elevation[b]	Factor
Pt/Cr (Xtal/Xtal)	3.5	11.5 GPa	3.8 GPa[a] 556 ksi	~10 X
304SS/Zr (Xtal/Am)	2.72	9.3 GPa	3.1 GPa[a] 450 ksi	~8 X
Cu/Zr (Xtal/Am)	**40**	**2.7 GPa**	**≈1.1 GPa[b] 152 ksi**	**~5 X**
Cu/304SS (Xtal/Xtal)	2.0	5.2 GPa	1.68 GPa[b] 243 ksi	~4 X
Cu/Monel (Xtal/Xtal)	2.0	4.4 GPa	210 ksi[b]	~3.5 X

[a] Estimated from hardness measurements,
[b] Measured in standard tensile tests ($\varepsilon = 5 \times 10^{-5}$/sec)

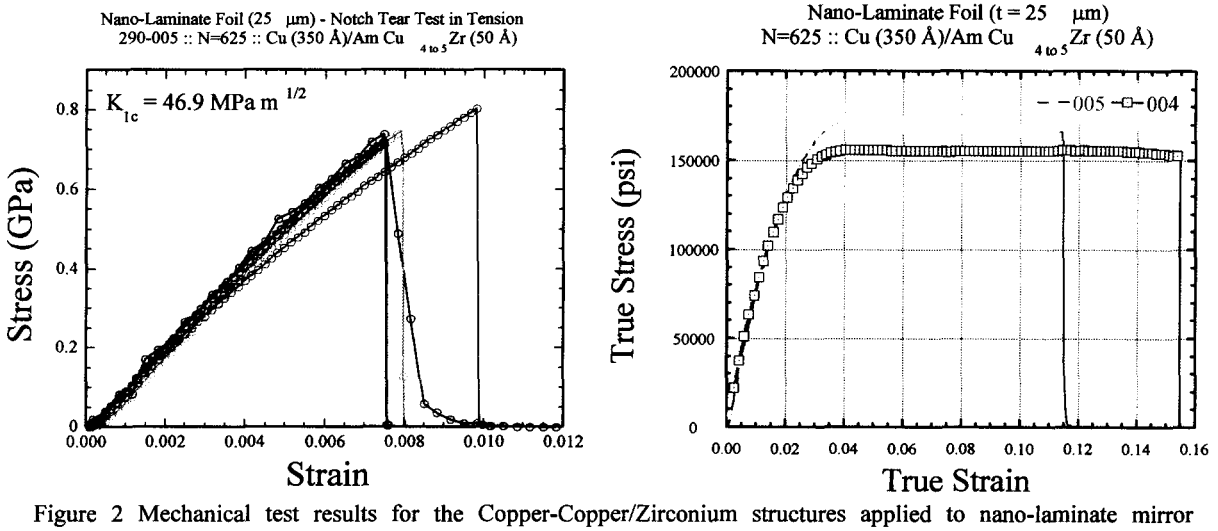

Figure 2 Mechanical test results for the Copper-Copper/Zirconium structures applied to nano-laminate mirror development are presented. The data are from low strain rate laboratory mechanical tests using foil samples. The Young's modulus of this Cu/Zr nano-laminate was determined to be $E \approx 14 \times 10^6$ psi.

The mechanical properties of a 25 μm thick Cu/Zr nano-laminate (Cu – 350 Å : Cu_3Zr – 50 Å) are presented in Figure 2. The tear fracture toughness is consistent with values obtained for mild steel having the same ultimate tensile strength. The elastic-perfectly plastic mechanical response of this nano-laminate is worth pointing out as it is not characteristic of the two component materials in elemental form.

2.4 Nano-Laminate Mirror Synthesis

Developmental work on nano-laminate fabrication was done using flat twenty-five cm and fifty cm diameter float glass substrates. This material was selected on the basis of cost, availability and surface roughness. Measured surface roughness on the float glass flats ranged from 12 Å to 20 Å and was replicated by the deposited nano-laminate foils.

Approximately fifty foils were fabricated on float glass in this development phase. More than fifteen twenty-five cm diameter nano-laminate mirror foils have been fabricated using figured super-polished ($\sigma \approx$ 10 Å) Zerodur substrates. More than eight fifty cm diameter nano-laminate foils have been fabricated using

figured super-polished ($\sigma \approx 10$ Å) Zerodur substrates. The Zerodur substrates were not damaged and only required cleaning prior to reuse. Synthesis processing time varied from 36 to 96 hours depending on the design nano-laminate thickness. The surface quality of these nano-laminate structures is dependent on the quality of the substrates used. Measurement of surface roughness of the nano-laminate foil surfaces in contact with the Zerodur tooling substrates after parting from the tooling have shown that this surface replicates the roughness of the Zerodur - ($\sigma \approx 10$ Å.)

Figure 3: The 33 inch inside diameter sputter deposition chamber used in this work is shown. The two 8 inch dia. magnetron sources (Cu and Zr) are mounted 180 degrees apart. Substrates are mounted 3 to 6 inches above the planar magnetrons and rotated about the center of the chamber, layers being deposited as substrates pass over each magnetron source. Mounting configurations for the 25 cm and 50 cm diameter substrates is shown in Figure 4.

The deposition system was equipped with three sputter magnetron deposition sources: two 8 inch diameter circular planar sources for copper and zirconium and one 4 inch diameter circular planar magnetron for carbon. The carbon was deposited first and acted to enhance parting of the fabricated nano-laminate foils from the substrate tooling. Layering was accomplished by mounting the substrates on a table continuously rotating about its center. This table was center on the axis of the circular vacuum chamber shown in Figure 4. The 25 cm and 50 cm diameter substrates were rotated at 100 rpm about their centers as they were rotated over the 8 inch diameter sources to improve foil thickness uniformity. Thickness uniformity for this deposition system was ± 5%.

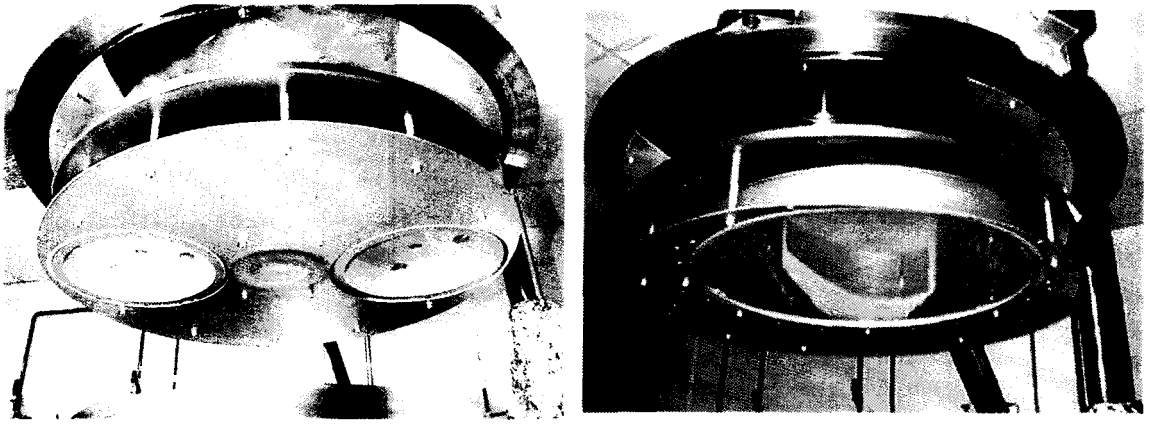

Figure 4. The mounting arrangements for the 25 cm and 50 cm diameter substrates are shown. Two 25 cm nano-laminates were synthesized in one fabrication process experiment. The substrates were rotated about there centers at 100 rpm during the full synthesis run to enhance nano-laminate thickness uniformity.

It is well known that the magnetron sputter deposition characteristics of materials in elemental, alloy or inter-metallic forms vary widely. Engineering calibration of process parameters for the range of materials to be used are defined by experiment. Important nano-laminate structural and fabrication process characteristics include: 1) layer thickness; 2) layer thickness uniformity throughout a sample; 3) layer composition; 4) fabrication process reproducibility; 5) fabrication process stability in a long deposition experiment; 6) fabrication process flexibility etc. Therefore, a systematic approach to the development of a nano-laminate magnetron sputter deposition process is needed if the structural and fabrication process characteristics outlined above are to be reproducibly achieved.

Four basic characteristics of magnetron sputtering and the technology applied here make this possible. First, excitation of magnetron sputter deposition sources is primarily with very stable direct current electrical power supplies: stability at the one part in ten thousand is available. Second, the integrated sputtering rate (atoms/unit time) of a given material in a given source geometry is empirically known to be nearly linearly dependent on the sputter source excitation power and to be very reproducible given the power applied is reproducible. Third, stable, one part in ten thousand, motion control is available. Fourth, individual layer thickness is determined by passing a substrate through the full deposition field of a sputter source thus taking advantage of the first three factors presented above.

The thickness of the layers ($t_{A,B}$ – Å) deposited onto the substrates rotated over the deposition sources is parametrically related to the rotation period of the large table (τ - sec) and the deposition rate of each material onto a fixed substrate directly over each source ($R_{A,B}$ – Å/sec) by

$$t_{A,B} = \tau \, R_{A,B} \, K \qquad (Å) \qquad (1)$$

where K is an empirically determined constant relating layer thickness to deposition rate $R_{A,B}$ for a given τ. K characterizes the relationship of the total sputtering rate (atoms/unit time) to the thickness of materials A or B deposited as a sample passes through the full deposition field of sputter a source. K can also be calculated using models of the deposit thickness distribution characteristic of a given magnetron sputter source. Additionally, the deposition rate $R_{A,B}$ is, to an excellent approximation, linearly dependent on the power supplied to the sputter source ($P_{A,B}$ - watts) as expressed below:

$$R_{A,B} = k \, P_{A,B} \, . \qquad (2)$$

Substituting EQ. (2) into EQ. (1) yields

$$t_{A,B} = \tau \, k \, P_{A,B} \, K. \quad (Å) \qquad (3)$$

Eq. (3) is then used to calculate the experimental parameters τ, and $P_{A,B}$ required to fabricate a nano-laminate design containing layers A and B having thickness t_A and t_B. A more efficient approach is to experimentally determine the product kP_AK by depositing a sample of total thickness T_A of materials A alone containing N layers from a source excited at a power of P_A. Eq. (1) is then used to determine the parameter kP_AK using the thickness of a single layer $t_A = T_A/N$. Since k and K are constants the relationship between t_A, τ and P_A is determined and nano-laminate synthesis run parameters required to fabricate a given sample design can be calculated. This approach is used to determine the nano-laminate deposition process parameters. Typical synthesis process parameters are presented in Table 3.

Table 3. The Range of Nano-Laminate Process Parameters Applied is Presented

Table Rotation Period	τ = 240/120/60 sec
Substrate Rotation Period	t = 0.6 or 0.3 sec
Fabrication Time	t ≈ 24 to 120 hours.

Copper Power	250 to 650 watts
Zirconium Power	50 to 150 watts
Carbon Power	250 to 500watts
Argon Pressure	1.5 to 4.5 μm

A 25 cm diameter, 110 μm thick thin shell mirror consisting of alternating 600 Å thick copper layers and 80 Å thick copper/zirconium amorphous intermetallic layers is shown in Figure 5 with a 50 cm diameter sample still adhered to its flat float glass tooling. A surface finish of 10 Å achieved using a super-polished Zerodur 25 cm diameter tool. The surface finish of the 50 cm float glass tool part was ≈ 18 Å.

25 cm diameter on Zerodur **50 cm diameter on Float Glass**

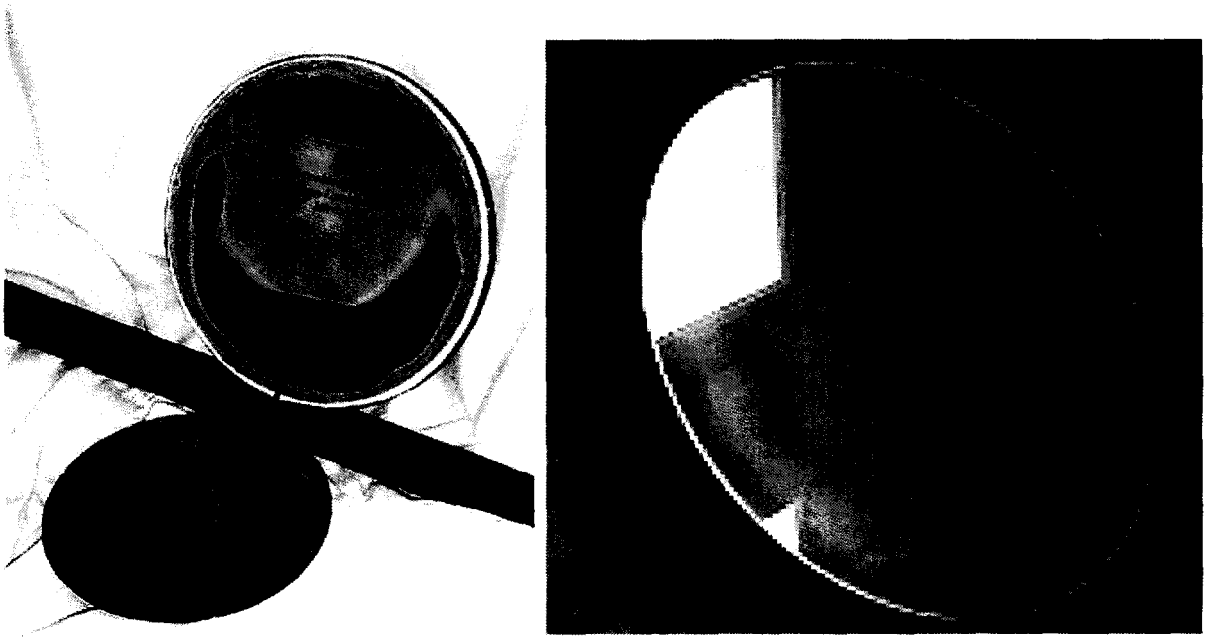

Figure 5. A 25 cm diameter, 110 μm thick thin shell mirror consisting of alternating 600 Å thick copper layers and 80 Å thick copper/zirconium amorphous intermetallic layers is shown . A surface finish of 10 Å achieved off a super-polished tool. A 50 cm diameter CuZr nano-laminate still adhered to its float glass substrate is also shown.

Samples of both 25 cm and 50 cm diameter copper/zirconium nano-laminate mirror foils fabricated on flat float glass tooling, on 25 cm diameter super-polished Zerodur concave figured substrates and 50 cm diameter super-polished Zerodur concave figured substrates have been rim supported and parted from their tooling substrates. These flat, concave and convex rim supported nano-laminate mirror structures have received moderate characterization. The flat 25 cm diameter samples are flat to 1.5 to 2 waves replicating the float glass tooling figure. These samples have smoothness that replicates the float glass smoothness, $\sigma \approx$ 12 to 20 Å. The figured tooling samples exhibit smoothness that replicates the super-polished Zerodur, $\sigma \approx$ 10 Å. These figured foils are very flexible and require support for figure measurements to be undertaken. This work is underway in conjunction with the Jet Propulsion Laboratory in the Actuation System and Modeling development component of this program.

2.5 Nano-Laminate Mirror Development Conclusions

The work presented here has shown that high fidelity replication of large area (490 cm^2 and 980 cm^2) near atomically smooth float glass and super-polished Zerodur substrate tooling can be reproducibly carried out using thin foil (25 μm to 120 μm thick) nano-laminate technology. These thin nano-laminate foils have

exceptional mechanical properties which enable handling and is expected to make possible actuation of figured tooling fabricated foils to achieve the desired figure. Though the work to date has extended the scale of high fidelity replication technology for optic applications by more than a factor of four our goals are much more aggressive.

TABLE 4: Nano-Laminate Development needs for Production of a 2 meter diameter, 0.1 micron rms surface figure Nano-laminate Thin Shell Mirror structures

Technology Area	Technology Needs	Drivers	Limiting factor
A. Materials Development of Properties Database	▪ Develop materials systems reducing areal weight and enabling surface figure optimization via thermal reaction/ internal stress reduction on master tool before parting thin shell optic structure ▪ Thin shell optic structures in the thickness range of 150 to 250 microns for mechanical stability	▪ Materials Science R&D ▪ Process demonstration	$/Time $/Time
B. Replication/Deposition of 2 meter Nano-laminate Thin Shells	▪ Uniform deposition over large figured substrate areas ▪ Minimization of residual stress in large surface area thin shell optic structures • Extend Thin Shell Optic foil parting technology to removal of very large area structures from tooling substrates	▪ Large deposition facility ▪ Demonstrate Process	$/Time; System design
C. Tooling substrate development	▪ Need lightweight 2 and 3 meter master substrate tooling to reduce thermal mass and to facilitate thin shell optic processing ▪ Potential materials are "thin" ULE /SiC/Foams supported by light weighted structures.	▪ Tool cost/ availability ▪ Radius of curvature of primary optic	$/Time

A concise summary of the technical areas required for Nano-Laminate development for a 2 meter diameter, 0.1 micron rms surface figure Nano-laminate Thin Shell Mirror is presented in Table 4. We believe that this nano-laminate work has established a technical basis for and taken the first steps in the development of a new paradigm for the creation of light weight-large area reflecting optic structures. Substantial research and development effort will be required to bring this to fruition as outlined in Table 4.

3.0 ACTUATION SYSTEMS AND MODELING DEVELOPMENT

The actuation system and modeling development is being conducted in parallel with the nanolaminate materials development. This work is in two parts, first is the electrostrictive actuation development and the second is the modeling effort needed for the characterization and control of the actuation system. The work will be presented first, followed by the modeling development.

Distributed piezoelectric actuator patches bonded on structures are used for active precision shape control of thin nanolaminate structure. The desired deformation field in the structure is obtained through the application of localized actuation forces and moments generated by expanding or contracting bonded

piezoelectric actuators. A newly developed formulation and numerical example to predict the response of shallow spherical aperture subjected to excitation from surface-bonded induced strain actuators were carried out in the research. This will be presented in brief. A full description of the mechanical modeling is being published in Reference [12].

The modeling of a piezoelectric actuated thin shell requires the modeling of first the electrical response of the piezo electric film. This then needs to be integrated and solved with the nonlinear mechanics of the thin shell. The general constitutive equations of piezoelectric material can be expressed as

$$T_{ij} = c^{D}_{ijkl} S_{kl} - h^{\theta}{}_{mij} D_m - \lambda^{D}_{ij} \theta$$
$$E_n = -h^{\theta}_{nkl} S_{kl} + \beta^{\theta S}_{nm} D_m - \nu^{S}_{n} \theta$$
$$\sigma = \lambda^{D}_{kl} S_{kl} + \nu^{S}_{m} D_m + a^{SD} \theta$$

where $\boldsymbol{S}$ is strain, $\boldsymbol{T}$ is stress, E is the electric field, D is the electric displacement, σ is entropy density, and θ is the dimensionless temperature [13]. The parameters c, h, β, ν, λ, a are the associate material constants. The superscripts S, D, or θ followed by the designate material constant indicates the condition of constant volume, constant electric displacement or constant temperature, respectively.

The general governing equations and boundary conditions can be expressed as the variation form

$$\delta\Pi(u_i, v) = \int (T_{ij}\delta S_{ij} - D_i \delta E_i - \delta u_i f_i^B + \delta v q^B) dV - \int_{S_f} \delta u_i f_i^{S_f} dS + \int_{S_q} \delta v q^{Sq} dS = 0$$
$$E_i = -v_{,i}; \quad u_i = u_i^{Su} (on\ Su), \quad v_i = v_i^{Sv} (on\ Sv)$$

Simplified constitution equations and the equation of motions can be obtained through the above equations by thin shell assumption [15-19].

3.1 Control and Shape Correction

For this paper, a nonlinear model for shell structures excited harmonically with induced strain actuator surface bonded patches was developed following the approach of Tzou *et al* [16]. Assume there is a distributed actuator layer laminated on the surface of the spherical shell and the actuator layer is bi-axially sensitive material. The distributed actuator patch is defined by the coordinates ϕ_1^*, ϕ_2^* in the meridional direction and ψ_1^*, ψ_2^* in the circumferential direction as shown in Figure 6.

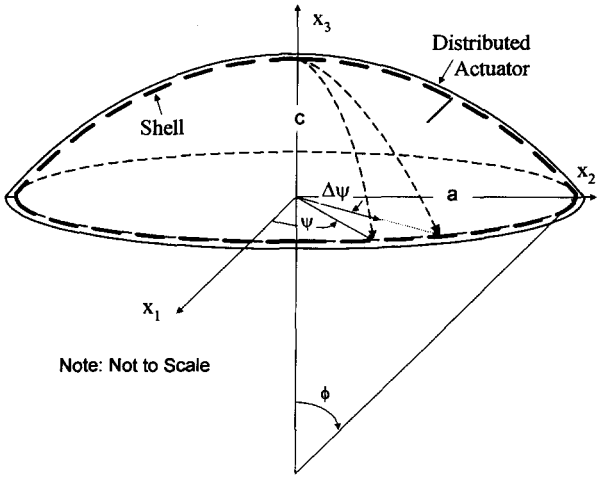

Figure 6: A thin hemispherical shell with a distributed patch actuator.

A control voltage ϕ^a, either open-loop or closed-loop, defines the magnitudes of distributed control forces N_{ii}^c and control moments M_{ii}^c induced by the actuator patch, i.e.,

$$N_{ii}^c = Y^a d_{3i} \phi^a \cdot U_s(\phi) \cdot U_s(\psi) ,$$
$$M_{ii}^c = r_i^a \left[h^a Y^a d_{3i} \phi^a \cdot U_s(\phi) \cdot U_s(\psi) \right],$$

where $i = \phi$ or ψ; Y^a is the actuator elastic modulus; d_{3i} is the piezoelectric constant; r_i^a s the distance measured from the neutral surface to the mid-surface of the actuator layer and $r_i^a = (h + h^a)/2 \approx h/2$, if h (the shell thickness)>>h^a (the actuator thickness); $\mathbf{U_S(a_i)}$ is a ***patch function*** and $\mathbf{U_S(a_i)}$ = $u_s(a_i - a_{i1}^*)$- $u_s(a_i - a_{i2}^*)$ where u_S is the ***unit step function*** (i,j = ϕ or ψ and $\phi = \phi_1^*, \phi_2^*$ or $\psi = \psi_1^*, \psi_2^*$). Thus, the system equation of the spherical shell coupled with the distributed actuator layer can be expressed as

$$(N_{\phi\phi} \sin\phi)_{,\phi} + N_{\psi\phi,\psi} - N_{\psi\psi} \cos\phi + \left[(M_{\phi\phi} \sin\phi)_{,\phi} + (M_{\psi\phi})_{,\psi} - M_{\psi\psi} \cos\phi \right] / R + Rq_\phi \sin\phi - R \sin\phi \, \rho h \ddot{u}_\phi$$
$$= (N_{\phi\phi}^c \sin\phi)_{,\phi} - N_{\psi\psi}^c \cos\phi + \left[(M_{\phi\phi}^c \sin\phi)_{,\phi} - M_{\psi\psi}^c \cos\phi \right] / R,$$

$$(N_{\phi\psi} \sin\phi)_{,\phi} + N_{\psi\psi,\psi} + N_{\psi\phi} \cos\phi + \left[(M_{\phi\psi} \sin\phi)_{,\phi} + M_{\psi\psi,\psi} + M_{\psi\phi} \cos\phi \right] / R + Rq_\psi \sin\phi - R \sin\phi \rho h \ddot{u}_\psi$$
$$= N_{\psi\psi,\psi}^c + M_{\psi\psi,\psi}^c / R,$$

$$\left[(M_{\phi\phi} \sin\phi)_{,\phi} + M_{\psi\phi,\psi} - M_{\psi\psi} \cos\phi \right]_{,\phi} / R + \left[[(M_{\phi\psi} \sin\phi)_{,\phi} + M_{\psi\psi,\psi} + M_{\psi\phi} \cos\phi)] / \sin\phi \right]_{,\psi} / R$$
$$- (N_{\phi\phi} + N_{\psi\psi}) \sin\phi + Rq_3 \sin\phi - R \sin\phi \, \rho h \ddot{u}_3$$
$$= \left[(M_{\phi\phi}^c \sin\phi)_{,\phi} - M_{\psi\psi}^c \cos\phi \right]_{,\phi} / R + [M_{\psi\psi,\psi}^c / \sin\phi]_{,\psi} / R - (N_{\phi\phi}^c + N_{\psi\psi}^c) \sin\phi .$$

where N_{ij} are the membrane forces; M_{ij} are the bending moments; R is the radius; ρ is the mass density; h is the shell thickness; q_i is the external excitation; u_i are the displacements in the ith direction. The first two equations define the meridional and the circumferential directions, and the last one defines the transverse system equations. Distributed control components appear in all three equations and thus, open- or closed-loop distributed control of spherical shells can be achieved. Note that there are the three fully coupled spherical shell/actuator system equations. Due to the complexity of the shell equations, assumptions and simplifications are often employed. There are three approximation theories used inythis analysis, namely, 1) the bending approximation (or the inextensional approximation), 2) the membrane approximation (or the extensional approximation), and 3) the Donnell-Mushtari-Vlasov approximation. Accordingly, based on shell definitions and assumptions, one can further simplify these three system equations to accommodate various practical applications, e.g., control of membrane shells, etc. Detailed of the derivation can be found in [12] and are omitted here for brevity.

3.2 Case Study:

Piezoelectric material patched to the back surface of the mirror are used as the local precision control element. These piezoelectric patches are consisting sectors or separate strips with control electrodes. Table 5 shows a typical PV range of Seidel aberrations for a 100mm aperture mirror where r is radius, ψ_0 is the reference angle, A_D, A_S, A_G, and A_C are the amplitude parameters for defocusing, spherical aberration, astigmatism, and coma, respectively. The properties of a copper-copper/zirconium nanolaminate with 25 cm 100μm thick aperture, and focal ratio F = 1/8 is used in the numerical example.

Table 5. The PV range of Seidel aberrations for a 100mm aperture mirror.

Aberration	Representation	PV, micron
Defocusing	$A_D r^2$	10.8
Spherical aberration	$A_S r^4$	3.5
Astigmatism	$A_G r^2 \cos(\psi+\psi_0)$	0.55
Coma	$A_C r^2 \cos(\psi+\psi_0)$	0.47

As shown in Table 5, these and other kinds of aberration need to be corrected through an optimal design of the arrangement of actuators and a practical control mechanism. For the following examples, a finite element model is used to evaluate the control provided by PVDF actuator patches as indicated in each of the figures below.

Following cases shown in Figures 7-9 shows the contour plots of the nanolaminate shell actuated with a voltage of +168 volt. The left hand side is the actuated actuator patch(es), the right hand side is the calculated response of the normal displacement of the surface.

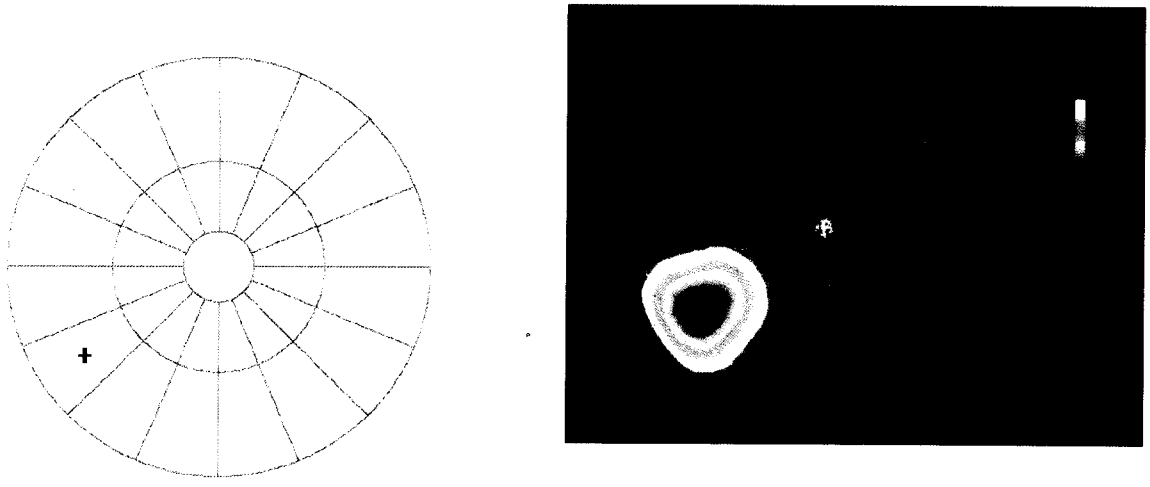

Figure 7: Voltage applied to a single electrode.

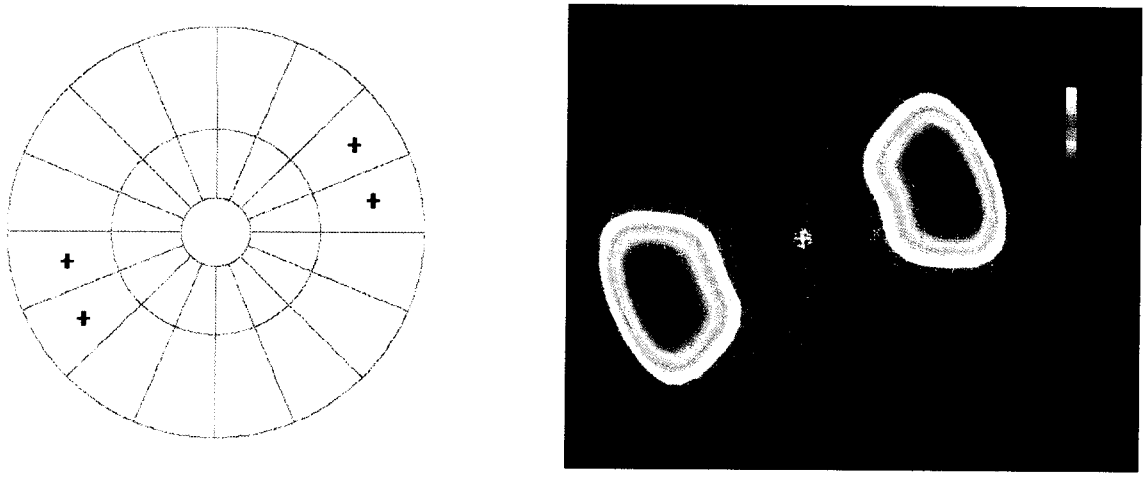

Figure 8: Voltage applied to symmetric and opposite electrodes.

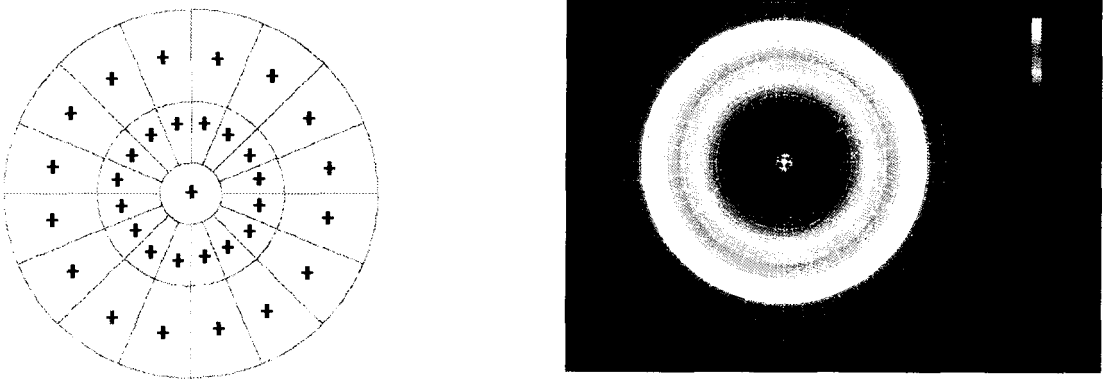

Figure 9: Voltage applied to all the electrodes (defocus)

3.3 Distributed control of thin membrane shell

The analytical distributed control of nonlinear thin membrane shell continua has developed and is presented in detail in the references [13,18]. Based upon the thin shell model, the modal responses of nonlinear membrane shell continua can be independently controlled. From this the application fundamental theories, distributed control mechanisms and solution procedures and the resulting derived generic nonlinear membrane shell continuum results can be easily and widely applied to a thin shell structure. This allows the development of preliminary design concepts based on the assembly of unit cells, and distributed local and global actuation and control of membrane structures that can be carried out both analytically and experimentally. Figure 10 shows a special designed micro-cells assemblage of the actuators. The unit cell in the design is composed of four strip-like actuators with off-axis arrangement to perform bending and twisting forces for a special adjustment of localized aberration.

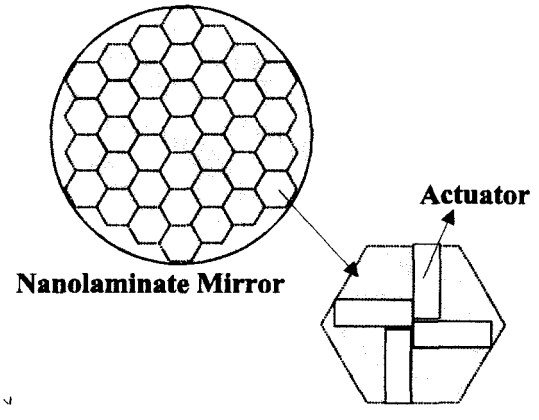

Figure 10: Array of distributed actuators based on a unit cell on a thin shell membrane

A preliminary study has been performed to study the influence function of the unit actuators cell with finite element analysis is shown in Figure 11. The numerical results are shown, where the influence function with perspective and cross section views are presented as in the right top and bottom of the figure. The results show the maximum displacement is around 7.5 micron with a 300 Volts DC input. This modeling effort has been verified with experimental testing.

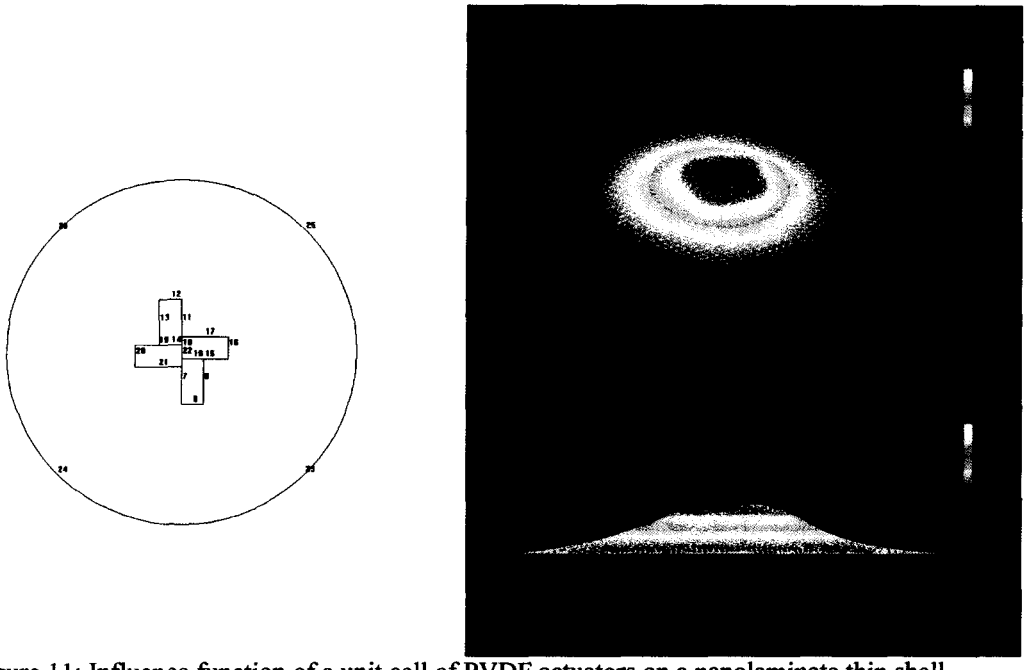

Figure 11: Influence function of a unit cell of PVDF actuators on a nanolaminate thin shell.

4.0 SUMMARY

Nanolaminate materials are presented as a new class of materials for optics including large actively controlled telescope systems. They represent the most mature nanostructured materials available with the capability to approach theoretical limits strength and increased stiffnesses representative of metallic materials. This approach to replicated optics reduces cost and time to delivery, and is scalable to large area optical reflector surfaces. This enables a new class of thin shell optics that allows for precision in-plane actuation with areal densities approaching 2 kg/m2 including actuation. This technology is scalable to several meters in diameter and lends itself to rapid manufacture of precision replicated, low scatter optics. This technology when combined with electroactive actuation is enabling technology for ground based astronomy and many future NASA missions, such as Terrestrial Planet Finder.

ACKNOWLEDGEMENT

Parts of this research were carried out at the Jet Propulsion Laboratory, California Institute of Technology, under a contract with the National Aeronautics and Space Administration as well as performed under the auspices of the U. S. Department of Energy by the University of California, Lawrence Livermore National Laboratory under Contract No. W-7405-Eng-48. Reference herein to any specific commercial product, process, or service by trade name, trademark, manufacturer, or otherwise, does not constitute or imply its endorsement by the United States Government or the Jet Propulsion Laboratory, California Institute of Technology. Authors would also show the appreciation of Prof. H. S. Tzou and his associates from University of Kentucky for their inputs for the modeling work.

REFERENCES

1. T. W. Barbee, Jr., "Multilayer Structures: Atomic Engineering in its Infancy," *in Physics, Fabrication and Applications of Multilayered Structures*, Proc. of a NATO Advanced Study Institute (New York, NY, 1988) p. 17-32.
2. T. W. Barbee, Jr., F. Spaepen, and L. Greer, eds. *Multilayers: Synthesis, Properties and Non-Electronic Applications (Symposium)*, Mater. Res. Soc. Conf. Proceedings Vol. 132 (Boston, MA, 1987).
3. Troy W. Barbee, Jr., "Nano-structure Multilayer Materials", in *State of the Laboratory,* Lawrence Livermore National Laboratory, UCRL-5200-91-718 (1991).
4. 1976 National Science Foundation Report to the United States Congress,, "Development of Multilayer

Synthesis Technology" by T. W. Barbee, Jr. in the Center of Materials Research at Stanford University selected as one of four major achievements in Materials Research resulting from programs funded by the Materials Office of the National Science Foundation during FY1976.

5. T. W. Barbee, Jr. and D. L. Keith, "Synthesis of Metastable Materials by Sputter Deposition Techniques," Proc. at the Fall Meeting of the Metallurgical Society of AIME, Pittsburgh, PA, October 5-9, 1980
6. T. W. Barbee, Jr., "Multilayer Synthesis by Physical Vapor Deposition," in *Synthetic Modulated Structures* , ed. by L. Chang and B. C. Giessen, (Academic Press, New York, 1985), pp. 313-337
7. Troy W. Barbee, Jr., "Atomic Engineering" in *Science and Technology Review*, Lawrence Livermore National Laboratory, UCRL 5200-97-12, (1997).
8. T. P. Weihs, T. W. Barbee, Jr. and M. A. Wall, "A Low Temperature Technique for Measuring Enthalpies of Formation", *J. Mater. Res.*, Vol. 11(6), 1403-1409 (1996); T. P. Weihs, T. W. Barbee, Jr. and M. A. Wall, "Hardness, Ductility and Thermal Processing of Cu/Zr and Cu/Cu-Zr Nanoscale Multilayer Foils", *Acta mater.* **45**(6), 2307-2315 (1997); T.D. Nguyen and T.W. Barbee, Jr., "Mechanical Properties of Cu/Ta Multilayers Prepared by Magnetron Sputtering", MRS Proc.Vol. 522, 295 (1998).
9. T.W. Barbee, Jr., "Sputtered layered synthetic microstructure (LSM) dipersion elements," Proceedings of the Topical Conference on Low Energy X-Ray Diagnostic, (Monterey, CA.), June 8-10, 1981, pp. 131-45.
10. T. W. Barbee, Jr., "Multilayers for X-ray Optics", Opt. Eng. **25**, 898-915, (1986): T.W. Barbee, Jr., "Multilayers for X-ray Optical Applications," Springer Ser. Opt. Sci., 43 (X-Ray Microsc.), pp. 144-62 (1984)
11. T.W. Barbee, Jr., S. Mrowka, and M.C. Hettrick, "Molydenum-silicon multilayer mirror for the extreme ultraviolet," Applied Optics, 24(6), pp. 883-6 (1985) ; A. B. C. Walker, Jr., T. W. Barbee, Jr., R. B. Hoover, J. F. Lindblom, "Soft X-Ray Images of the Solar Corona with a Normal-Incidence Cassegrain Multilayer Telescope," Science, 241, pp. 1781-1787 (1988).
12. S.-S Lih, G. Hickey, J. H. Ding, and S. H Tzou, "Micro-Control Actions Of Segmented Actuators On Shallow Paraboloidal Shell Reflectors," ASME International Adaptive Structures and Materials Systems Symposium, New Orleans, 2002 (to appear).
13. R. D. Mindlin, "On the Equations of Motion of Piezoelectric Crystals," in *Problems of Continuum Mechanics*, Contributions in Honor of The Seventieth Birthday of Academician N. I. Muskelishvili, *the Society for Industrial and Applied Mathematics*, pp. 282-290., Feb. 1961
14. H.S.Tzou, *Piezoelectric Shells (Distributed Sensing and Control of Continua),* Kluwer Academic Publishers, Dordrecht/Boston/London., 1993.
15. H.S.Tzou,Y. Bao, and Venkayya, V.B., "Microelectromechanics and Functionality of Segmented Cylindrical Shell Transducers," *Structronic Systems - Smart Structures, Devices and Systems*, Volume-1, A. Guran and H.S. Tzou (Editors); G.L. Anderson and M.C. Natori, (Associate Editors), pp.151-196, World Science Publishing Co., Singapore. 1998.
16. H.S.Tzou and Y Bao, "Nonlinear Piezothermoelasticity and Multi-field Actuations, Part-1: Nonlinear Anisotropic Piezothermoelastic Shell Laminates," ASME *Journal of Vibration & Acoustics*. Vol.119, pp.374-381, 1997.
17. H.S.Tzou. and R.V. Howard, "A Piezothermoelastic Thin Shell Theory Applied to Active Structures," *ASME Transactions, Journal of Vibration & Acoustics*, Vol.116, No.3, pp.295-302, 1994.
18. Tzou, H.S. and R. Ye, "Piezothermoelasticity and Precision Control of Piezoelectric Systems: Theory and Finite Element Analysis," *ASME Transactions, Journal of Vibration & Acoustics*, Vol.116, No.4, pp.489-495, 1994.